N O T I C E

THIS DOCUMENT HAS BEEN REPRODUCED FROM MICROFICHE. ALTHOUGH IT IS RECOGNIZED THAT CERTAIN PORTIONS ARE ILLEGIBLE, IT IS BEING RELEASED IN THE INTEREST OF MAKING AVAILABLE AS MUCH INFORMATION AS POSSIBLE

NASA

Technical Memorandum 82048

Discovery of Natural Gain Amplification in the 10μm CO_2 Laser Bands on Mars: The First Definite Natural Laser

M. Mumma, D. Buhl, G. Chin, D. Deming,
F. Espenak, T. Kostiuk, and D. Zipoy

NOVEMBER 1980

National Aeronautics and
Space Administration

Goddard Space Flight Center
Greenbelt, Maryland 20771

DISCOVERY OF NATURAL GAIN AMPLIFICATION IN THE 10 μm CO_2 LASER BANDS ON MARS: THE FIRST DEFINITE NATURAL LASER

By

Michael J. Mumma, David Buhl, Gordon Chin, Drake Deming
Fred Espenak, Theodor Kostiuk

Infrared and Radio Astronomy Branch
Laboratory for Extraterrestrial Physics
NASA-Goddard Space Flight Center
Greenbelt, MD 20771

and

David Zipoy
Astronomy Program
University of Maryland
College Park, MD 20742

ABSTRACT

Fully resolved intensity profiles of various lines in the CO_2 bands at 9.4 μm and 10.4 μm have been measured on Mars using an infrared heterodyne spectrometer. Analysis of the line shapes shows that the Mars atmosphere exhibits positive gain on these lines, providing the first definite detection of natural optical gain amplification and enabling identification of these lines as the first definite natural laser ever discovered.

Since their invention some 25 years ago, optical lasers have become nearly ubiquitous tools in the laboratory and in everyday life (e.g. super-market price scanners). Despite this somewhat deceiving abundance of man-made lasers, no definite naturally-occurring lasers have ever been reported, even though the extreme variety of physical and chemical environments of extra-terrestrial objects plausibly argues that natural lasers must exist (1). Natural microwave amplifiers (masers) have been found to be abundant in interstellar clouds and some circumstellar shells, primarily among the rotational level populations of certain molecules (e.g. OH, SiO, H_2O), and are all characterized by the property $h\nu \lesssim kT$, where T is the kinetic temperature. However, optical lasers are characteristic of electronic or vibrational transitions for which $h\nu >> kT$. Many examples of natural non-thermal optical emission have been found, such as the infrared and ultraviolet aurorae and/or day glows of Earth, Jupiter, Mars, and Venus, but it has never been established that a population inversion exists for any of these emissions. The relative populations of the two molecular levels must be inverted in order for gain amplification to occur, the essence of lasing. We report here the discovery of a population inversion and natural gain amplification in the 10.4 μm CO_2 laser bands on Mars, representing to our knowledge the first definite identification of a natural infrared laser.

The observations were made with the Goddard infrared heterodyne spectrometer (2) during the period January-April, 1980 when the planet was near opposition. The beam size (HPBW) was 1.7 arc-sec and the disk of Mars was $\sim$ 13.8 arc-sec diameter, providing good spatial resolution on the planet. Fully resolved atmospheric line profiles were measured at various locations on the disk, including many individual rotational-vibrational lines in both the 10.4 μm ($00^0 1 - [10^0 0, 02^0 0]_I$) and 9.4 μm ($00^0 1 - [10^0 0, 02^0 0]_{II}$) bands. Analysis of the full set of lines is proceeding, and we report here some results obtained from analysis of several measurements of the 10.33 μm R8 line at 967.7072cm^{-1}.

The intensity profiles were measured simultaneously at 25 MHz (0.0008 cm^{-1}) resolution with 64 consecutive channels, and at 5 MHz (0.00016 cm^{-1}) resolution with a second bank of 64 consecutive channels.

It is important to note that all 128 channels were recorded simultaneously, thereby eliminating registration errors and drift. Absolute intensity calibration and removal of terrestrial atmospheric lines was achieved by lunar comparison spectra, measured nearly simultaneously and scaled to the appropriate air mass.

Fully resolved intensity profiles of the R8 line are shown (Fig. 1) for beams placed at disk-center, the north and south polar regions, and the equatorial east and west limbs (3). Several qualitative conclusions are evident by inspection of the spectra. First, in the absence of significant continuum opacity (local dust storms or clouds), the emergent intensity far from line center is a direct measure of thermal emission from the surface and therefore of the surface temperature. The measured surface temperatures agree well with data obtained by the Mariner 9 and Viking orbiters, where comparisons have been made to date. Second, analysis of the broad wings of the absorption line enables extraction of various atmospheric parameters by inversion of the radiative transfer equation for each location. Third, the bright emission at line center is evident at all positions with an intensity which is variable with location (4). It is this core emission which we will show constitutes a natural infrared laser.

Quantitative analysis of the disk-center spectra was performed in the following way. We first analyzed the line wings, from the continuum to within 50 MHz of line center. The solid surface temperature (typically 250K) was determined from the absolutely calibrated intensities far from line center. A discontinuity of 30K between the solid surface temperature and the gas temperature near the surface was assumed, in accord with radiative equilibrium and spacecraft observations (5). A mid-latitude model temperature profile typical of local noon, as determined by spacecraft measurements, was adopted and is shown in Fig. 2. A temperature lapse rate of 2.0 K/km was assumed to an altitude of ~45 km, followed by an isothermal atmosphere (typically 150K) above 45 km. The shaded portion of Fig. 2 represents the range of temperatures measured by the Viking probes in the so-called isothermal region (6) and the mean lapse rate is also in agreement with measurements

by Mars 6, and Viking for local noon (5).

We initially assumed that the ($00^{0}1$) state was in local-thermodynamic-equilibrium throughout the lower atmosphere ($z < 45$ km) and performed an iterative solution to the radiative transfer equation as a function of surface pressure. Two lines were well-fitted with these assumptions (e.g. Fig. 3a), however the remaining three lines showed too little atmospheric self-emission within $\sim$300 MHz of line center. No reasonable set of lapse rates, surface temperatures and pressures, or haze opacity produced a suitable fit for these three lines. However, all three remaining lines are well-fitted by the above described model if the ($00^{0}1$) source function is allowed to fall <u>below</u> the LTE value in the lower atmosphere of Mars. Furthermore, the vibrational relaxation rate coefficient derived in this way ($K \sim 4.7 \times 10^{-15} cm^{3} sec^{-1}$) agrees well with laboratory values (7). In addition, the retrieved surface pressures for all five lines agree well with the known values determined by the Mariner 9 topographic maps and the Viking Lander annual pressure measurements. We therefore believe that our observations represent the first observation of the failure of LTE in a planetary troposphere and we attribute this to screening of radiative exchange in the 4.3 μm band by airborne dust. Radiative energy exchange in a clear CO_2 atmosphere would keep the ($00^{0}1$) level in LTE to an altitude many scale heights above the level at which the collisional and radiative lifetimes were comparable (8), however a small amount of dust will efficiently capture quanta from the optically thick 4.3 μm band, thereby screening this exchange. It is beyond the scope of this paper to discuss this effect further, except to note that the detailed physics occurring in the troposphere does not significantly affect the principal conclusion of this paper. It is sufficient to note that we have successfully modelled the emergent tropospheric intensity, enabling us to strip this from the total emergent intensity, leaving the residual core emission.

Two fitted examples of the main lines are shown in Fig. 3. In addition to the calibrated single side-band experimental data we show separately the modelled self-emission of the lower atmosphere, the modelled transmitted surface intensity, and the sum i.e. the modelled

emergent intensity. We next stripped the modelled emergent intensity from the observed and fitted the residual core emission with a Gaussian profile, using a least-squares analysis for the amplitude, width, and velocity shift. Typical results are shown in Fig. 4.

The derived core emission line-widths are a direct measure of the kinetic temperature in the emitting region, and the integrated line brightness (E_8) can be related directly to the column density in the upper state ($00^0 1$) by the following relation:

$$N_{00^0 1} = \frac{4\pi E_8}{h\nu A_{10}} \frac{2J'+1}{J'} \frac{Q_{ROT}}{2(2J'+1)\exp(-\frac{B'hc\ J'(J'+1)}{kT})} \qquad (1)$$

where J' = 9, the rotational quantum number of the upper level of the R8 line. We assume the core emission to be emitted isotropically, which will be justified a-posteriori if the deduced atmospheric gain is sufficiently small that directional effects within the emitting region may be neglected. The effect of this assumption will be to underestimate the total atmospheric gain. We take the kinetic and rotational temperatures to be equal in the emitting region which has been shown to be peaked at ~75 km (4). The radiative transition rates (A_9, A_{10}) for the 9.4 μm and 10.4 μm bands have been measured in the laboratory (9). The rotational partition function (Q_{ROT}) may be taken to be 0.69 T/B to good approximation. The results of this analysis are given in Table I for five observations of the R8 line at disk center. We find that the column density in the ($00^0 1$) state is not less than 2.0×10^{14} cm^{-2} ± 2.0×10^{13} cm^{-2}.

We note that one line (Chryse Planitia) shows a substantially higher kinetic temperature (151K) than the remaining four observations which have a mean kinetic temperature of 113±10K. It's width (19.25 MHz) is nearly three standard deviations greater than the mean width of the other four lines (16.5±0.8). We have carried through parallel analyses based

on four and five lines respectively,because the Viking entry probes measured considerable thermal structure in the region 60-120 km suggesting that the observed high temperature (151K) may be real. We shall show that inclusion of this line in the analysis does not affect the main conclusion of this paper. We note that the total energy radiated in the 9 and 10 μm bands is 18.5 ergs $cm^{-2}s^{-1}$ which agrees well with earlier results (4). It is interesting to note that the energy radiated in the R8 line is $\sim 10^9$ times greater than would be radiated by this region of the atmosphere were it in local thermodynamic equilibrium.

The total directional gain, $\Gamma(\nu)$, along the line of sight may be calculated (10) from the relation

$$\Gamma(\nu) = \frac{\lambda^2}{8\pi} A_{10}\left(N_{J'} - N_{J''} \frac{w'}{w''}\right) g(\nu) \qquad (2)$$

where the w's are state statistical weights, and $g(\nu)$ is the line shape function. The emergent intensity will then be given by (for unsaturated amplified spontaneous emission) by

$$I(\nu = \eta(\exp \Gamma(\nu) - 1)$$

where η is some constant. If $N_{J'} > N_{J''} w'/w''$, the state populations are said to be inverted and the gain constant is positive definite, a necessary and sufficient condition for gain amplification (i.e. lasing) to occur.

We evaluate the maximum possible column density in the lower state $[10^{o}0, 02^{o}0]_I$ in the following way. We must establish three physical parameters, viz: (1) the base altitude level above which the emission originates, (2) the rotational temperature of the lower (I) level, and

(3) the vibrational temperature of the I level. The base altitude level may be established either by determining the region where the pumping energy is deposited, or more severely by requiring that the observed kinetic temperatures be greater than the condensation temperature. Johnson et al (4) have calculated the former, finding that ~50% of the core emission originates at altitudes greater than 75 km. We have independently verified their result. Condensation temperatures of 120 K and 113 K are reached at altitudes of 48 km and 65 km, respectively (6). We will show that a population inversion exists for each lower altitude bound, and therefore that the exact choice of altitude bound is unimportant for our main conclusion.

The vibrational exchange rate for I with $CO_2(00^0 0)$ is nearly gas kinetic (11) and the radiative relaxation rate is ~ 3 sec^{-1}. Therefore, collisional relaxation and radiative relaxation become comparable at ~120 km, far above the emitting region, and we expect collisions to dominate radiative effects at lower altitudes. We therefore take $T_{VIB} = T_{ROT} = T_{KIN}$, i.e. the I state must be in local thermodynamic equilibrium. We have already directly measured the kinetic temperature in the emitting region (Table I), and we may now calculate the maximum lower state (I) column density above our lower altitude bound for an exponential atmosphere. We find that in every case the lower state column density is less than the upper state column density (Table II), i.e. a population inversion exists.

We may now calculate the (minimum) directional gain at line center from:

$$\Gamma_o = \frac{\lambda_8^2}{8\pi} A_{10} \frac{J'}{2J'+1} \frac{2B}{0.69T} g(0)\left\{N_{00^0 1}(2J'+1)\exp\left(-\frac{B'hc}{kT} J'(J'+1)\right) - N_I(2J''+1)\frac{\nu'}{\nu''}\exp\left(-\frac{B''hc}{kT} J''(J''+1)\right)\right\} \quad (4)$$

where J" = 8, J' = 9, and the line-shape function at line center is

$$g(o) = \sqrt{\frac{\ln 2}{\pi}} \quad \frac{1}{\Delta\nu_D}$$

and we take $B_{00}{}^{o}{}_{1} = P_I = 0.39\ cm^{-1}$ (12).

The results are given in Table II. Note that when using the source function altitude bound, we have halved the upper state column density before calculating the gain. The gain is positive definite in all cases (13) and for the most reasonable lower bound (source function), the population inversion is greater than 50:1.

It is important to note that in every step we have routinely made assumptions which would minimize the total gain, nevertheless the derived gain is positive to an accuracy of ten standard deviations, based primarily on the accuracy with which the upper state population is determined (±10%). The derived gain would result in gain narrowing of the line by ~10 KHz, an unobservable amount compared with the kinetic line widths. However, the atmospheric gain should be substantially greater at large zenith angles than in the zenith direction and a search for macroscopic gain narrowing seems warranted.

In conclusion, natural gain amplification has been observed in the mesosphere of Mars, representing to our knowledge the first definite identification of a natural infrared laser.

References

1) Plausible candidates have been presented as possible natural lasers, including NH_3 10 μm emission from the Jovian polar regions (cf. T. Kostiuk, M. J. Mumma, J. J. Hillman, D. Buhl, L. W. Brown, J. Faris, and D. 1. Spears, Infrared Physics 17, 431 (1977); also M. J. Mumma, in "Proc. Intl. Conf. on Lasers '78", V. J. Corcoran, Ed. (STS Press, McLean, Va. 1979) p.700) and atomic hydrogen emission (Pfund β, near 4.65 μm) from the Becklin-Neugebauer infrared object (cf. H. Smith, H. Larson, and U. Fink, Ap. J. 233, 132 (1979). For a recent review of natural astrophysical masers, see L. E. Snyder, in "Interstellar Molecules", B. H. Andrew, Ed. (D. Reidel Co., Dordrecht (Holland), 1980).

2) A similar CO_2 laser - infrared heterodyne spectrometer is described in M. J. Mumma, T. Kostiuk, D. Buhl, Optical Engineering 17, 50 (1978). The heterodyne spectrometer was placed at the McMath Solar Telescope at Kitt Peak National Observatory. We thank Dr. Geoffrey Burbidge, Director for providing sufficient observing time, aand the Kitt Peak staff for excellent support. Kitt Peak National Observatory is operated by the Association of Universities for Research in Astronomy, under contract with the National Science Foundation. We also thank J. Faris, J. Guthrie, and C. Lowe of GSFC for excellent technical support.

3) The instrumental field-of-view was placed tangent to the planetary limb to minimize possible underfilling of the beam during measurements near the limb.

4) These bright core emissions were first reported in: M. A. Johnson, A. L. Betz, R. A. McLaren, E. C. Sutton, and C. H. Townes, Ap. J. (Letters) 208, L145 (1976). See also A. L. Betz, R. A. McLaren, E. C. Sutton, and M. A. Johnson, Icarus 30, 650 (1977). These authors

derived kinetic temperatures of 150-200K from the core emission line widths, much larger than the present results and substantially larger than the Viking probe data. However their observations accepted about twice the planetary area ours did, possibly leading to broadening of their observed lines by planetary rotation.

5) cf. "The Mars Reference Atmosphere", A. Kliore (ed.), COSPAR (Innsbruck, 1978), and references cited therein.

6) A. Seiff and D. B. Kirk, J. Geophys. Res., 82, 4364 (1977).

7) cf. J. C. Stephenson and C. B. Moore, J. Chem. Phys. 52, 2333 (1970).

8) R. E. Dickinson, J. Atmos. Sci. 29, 1513 (1972).

9) cf. E. R. Murray, C. Kruger, and M. Mitchner, Appl. Phys. Lett. 24, 180 (1974).

10) A. Yariv, "Quantum Electronics", John Wiley, New York (1975).

11) C. B. Moore, R. E. Wood, B. Hu, and J. T. Yardley, J. Chem. Phys. 46, 4222 (1967).

12) G. Herzberg, "Molecular Spectra and Molecular Structure II. Infrared and Raman Spectra of Polyatomic Molecules", Van Nostrand Reinhold Co., New York (1945).

13) We have also calculated the gain for a kinetic temperature of 151K corresponding to our 'high-temperature' line and find positive definite gain with the source function bound even for that case. However, were the temperature to be as high as 170K as observed by Johnson et al, we would find negative gain (absorption). We have also calculated the gain based on a mean Viking isothermal temperature of 140K and find positive gain for that case, as well.

FIGURE CAPTIONS

Figure 1 Partial Global Map of the CO_2 R8 Line on Mars. Small circles represent the placement and relative size of the instrumental field of view. Spectra are displayed with a linear intensity scale and 25 MHz (0.0008 cm^{-1}) spectral resolution. Note particularly the globally variable surface (continuum) temperatures, the (tropospheric) broad absorption line, and the (mesospheric) bright emission core. For clarity, we have omitted the higher resolution data near line center.

Figure 2 The model temperature profile used to analyse the broad absorption wings contributed mainly by the lower atmosphere. The altitudes at which the self-emission source function peaks for given frequency difference from line center are given on the right. Also shown are the two principal regions where the $(00^{\circ}1)$ state is found to depart from local thermodynamic equilibrium (LTE). P_I denotes the level for which the normalized source function falls to 0.5, P_{II} denotes the level for which the source function abruptly returns to LTE. The laser emission source function peaks at ~ 75 km.

Figure 3a R8 line profile near local noon over Chryse Planitia (CML 41°). The model requires LTE throughout the lower atmosphere to fit the emergent intensities from the continuum to within 50 MHz of line center, where the strong laser emission is seen. (,+ are 25 MHz; X are 5 MHz channels) data used to model the wing are marked as . The intensity scale is linear, relative to a 260K single side-band black body.

Figure 3b R8 line profile near local noon, north-west of Tharsis (CML 120°). A non-LTE model is required in the lower atmosphere to fit the line. An abrupt return to LTE at the 2.4 mbar level is found. In this case, the source function falls below 0.5 at 3.05 mbars. Intensity scale is linear, relative to a 266K single side-band black body.

Figure 4a Laser emission at the core of the R8 line over Chryse Planitia. The underlying curve is the total emergent intensity in the absence of laser emission, modelled as described in the text. The difference between the observed and modelled intensities is fitted to a gaussian as discussed in the text. Also shown are the half-width at half-maximum, the derived kinetic temperature, and the integrated energy in the laser line. Intensity scale is linear, relative to a single side-band 260K black body.

Figure 4b Laser emission north-west of Tharsis Montes. See text for discussion of analysis. Intensity scale is linear, relative to a single side-band 266K black body.

TABLE I. MARS: $^{12}C^{16}O_2$ R8 10.33μm Line @ Disk Center

CORE EMISSION ANALYSIS

BEAM CENTER LONGITUDE, LATITUDE	Observed HALF-WIDTH @HALF-MAX (MHZ)	APPARENT KINETIC TEMPERATURE (K)	OBSERVED LINE ENERGY[a] ergs $cm^{-2}s^{-1}sr^{-1}$	MINIMUM REQUIRED COLUMN DENSITY IN CO_2 $00^0 1$ STATE CM^{-2}
SE of Acidalia Planitia: 2°+24°	16.81	115.3	3.81(-2)	2.19(14)
Chryse Planitia: 41°+23°	19.25	151.1	4.46(-2)	3.03(14)
Tempe Fossae: 82°+25°	16.81	115.3	3.44(-2)	1.97(14)
NW of Thargis Montes: 120°+22°	15.51	98.1	3.93(-2)	2.07(14)
Amazonis Planitia: 158°+27°	17.39	123.4	2.87(-2)	1.71(14)
mean of 5:	17.15±1.36	[b] 120.0±19	3.70(-2) ±5.9(-3)	[c] 2.17(14) ±5.4(13)
mean of 4:	16.53±0.79	[b] 113±10	3.51(-2) ±4.8(-3)	1.99(14) ±2.0(13)

a) Corrected to the sub-solar point.

b) The condensation temperature (CO_2) is ~110K at 70 Km.

Viking temperature extremes (60-116 Km) were

V1 133.6K (92 Km) + 154.6 K (64 Km) 4:13 PM LMT

V2 115 K (116 Km) + 157 K (88 Km) 9:49 AM LMT

c) The integrated radiance in the 9 and 10μm bands is 18.5 ergs cm^{-2} s^{-1} at the sub-solar point.

TABLE II. MARS: CO_2 10.33μm RS TRANSITION:

Lower State Column Density and Atmospheric Gain

CONSTRAINT	LOWER ALTITUDE BOUND	T_K	COLUMN DENSITIES LOWER $[N_{020}, cm^{-2}]$	COLUMN DENSITIES UPPER $[N_{001}, cm^{-2}]$	MINIMUM POPULATION INVERSION (cm^{-2})	MINIMUM GAIN AT LINE CENTER
Condensation	48 Km	120K	$\leq 1.1 \times 10^{14}$	$\geq 2.2 \times 10^{14}$	+1.1(14)	+1.45(-3)
"	65 Km	113K	$\leq 4.0 \times 10^{12}$	$\geq 2.0 \times 10^{14}$	+2.0(14)	+ 2.71(-3)
Source Function	75 Km	120K	$\leq 3.2 \times 10^{12}$	$\geq 1.1 \times 10^{14}$	+1.1(14)	+ 1.38(-3)
"	75 Km	113K	$\leq 1.1 \times 10^{12}$	$\geq 1.01 \times 10^{14}$	+1.0(14)	+1.37(-3)

CONCLUSION: THE ATMOSPHERE EXHIBITS POSITIVE GAIN FOR ALL CASES.

NATURAL LIGHT AMPLIFICATION (LASING) IS OCCURRING ON MARS.

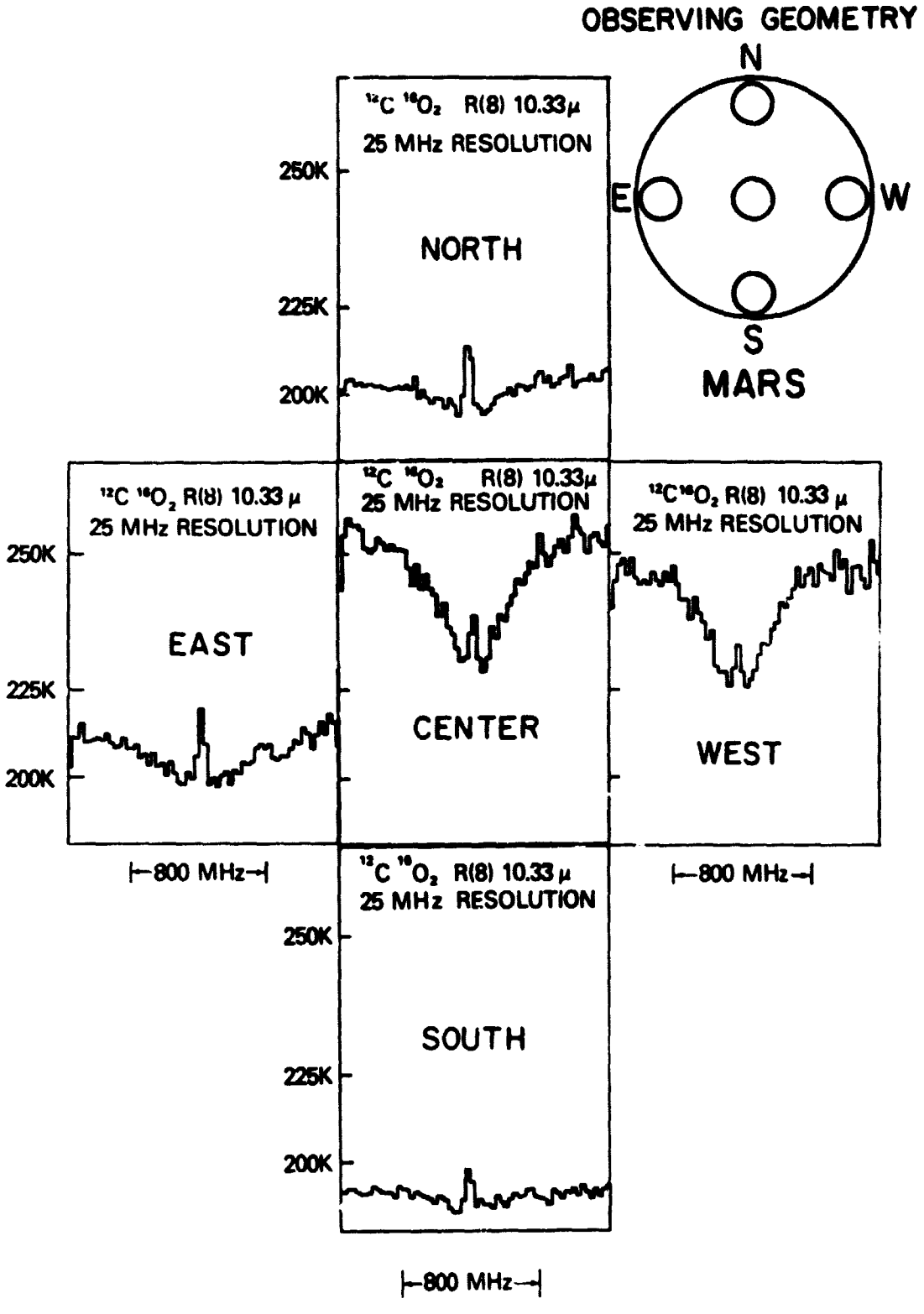

CO_2 LINE PROFILE MAP
OF MARS
FEB, 1980

FIGURE 1

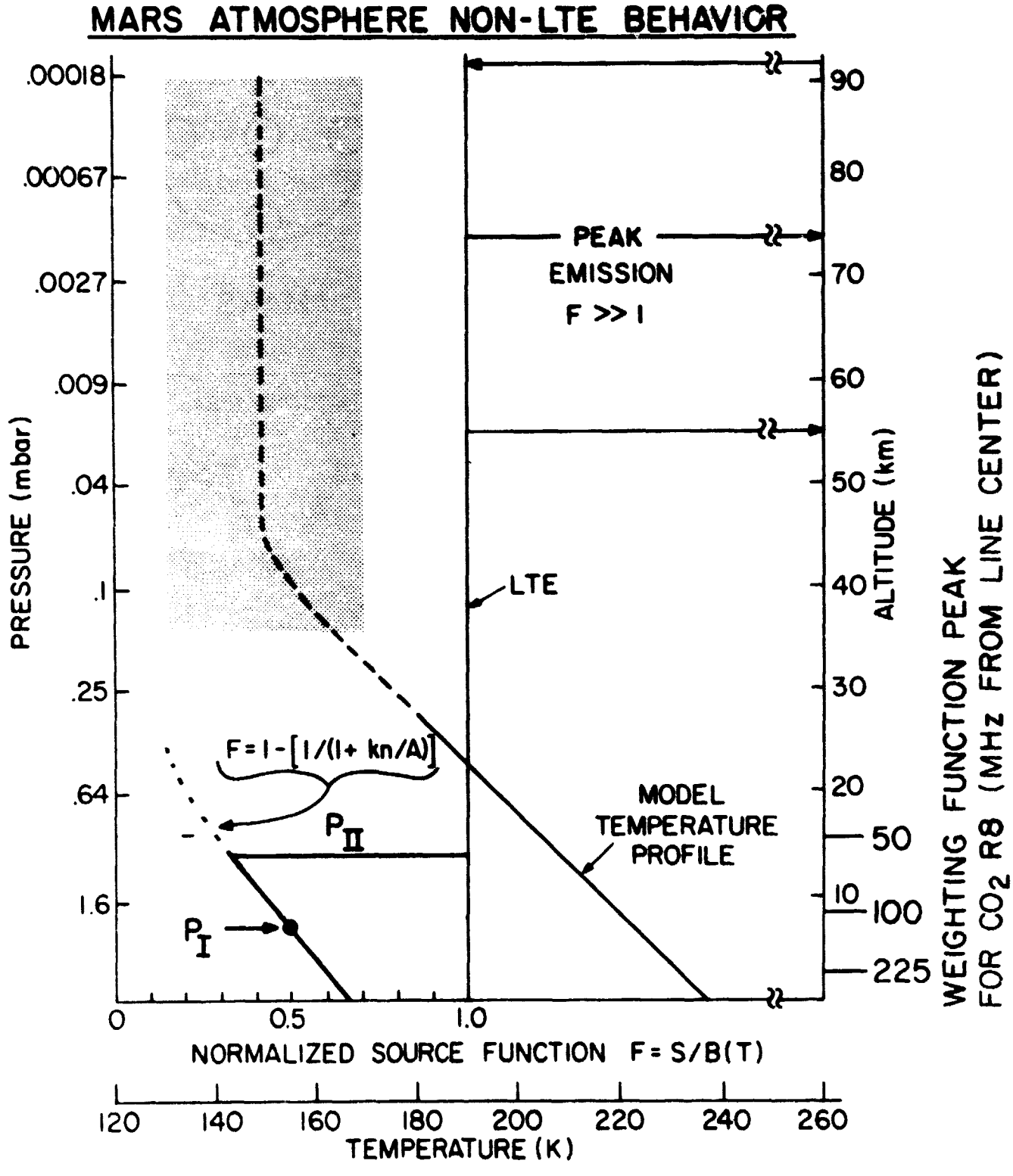
MARS ATMOSPHERE NON-LTE BEHAVIOR
.00018
.00067
.0027
.009
.04
.1
.25
.64
1.6
PRESSURE (mbar)
90
80
70
60
50
40
30
20
50
10
100
225
ALTITUDE (km)
WEIGHTING FUNCTION PEAK FOR CO_2 R8 (MHz FROM LINE CENTER)
PEAK EMISSION F >> 1
LTE
F = 1 - [1/(1+ kn/A)]
P_{II}
P_I
MODEL TEMPERATURE PROFILE
0
0.5
1.0
NORMALIZED SOURCE FUNCTION F = S/B(T)
120
140
160
180
200
220
240
260
TEMPERATURE (K)

FIGURE 2

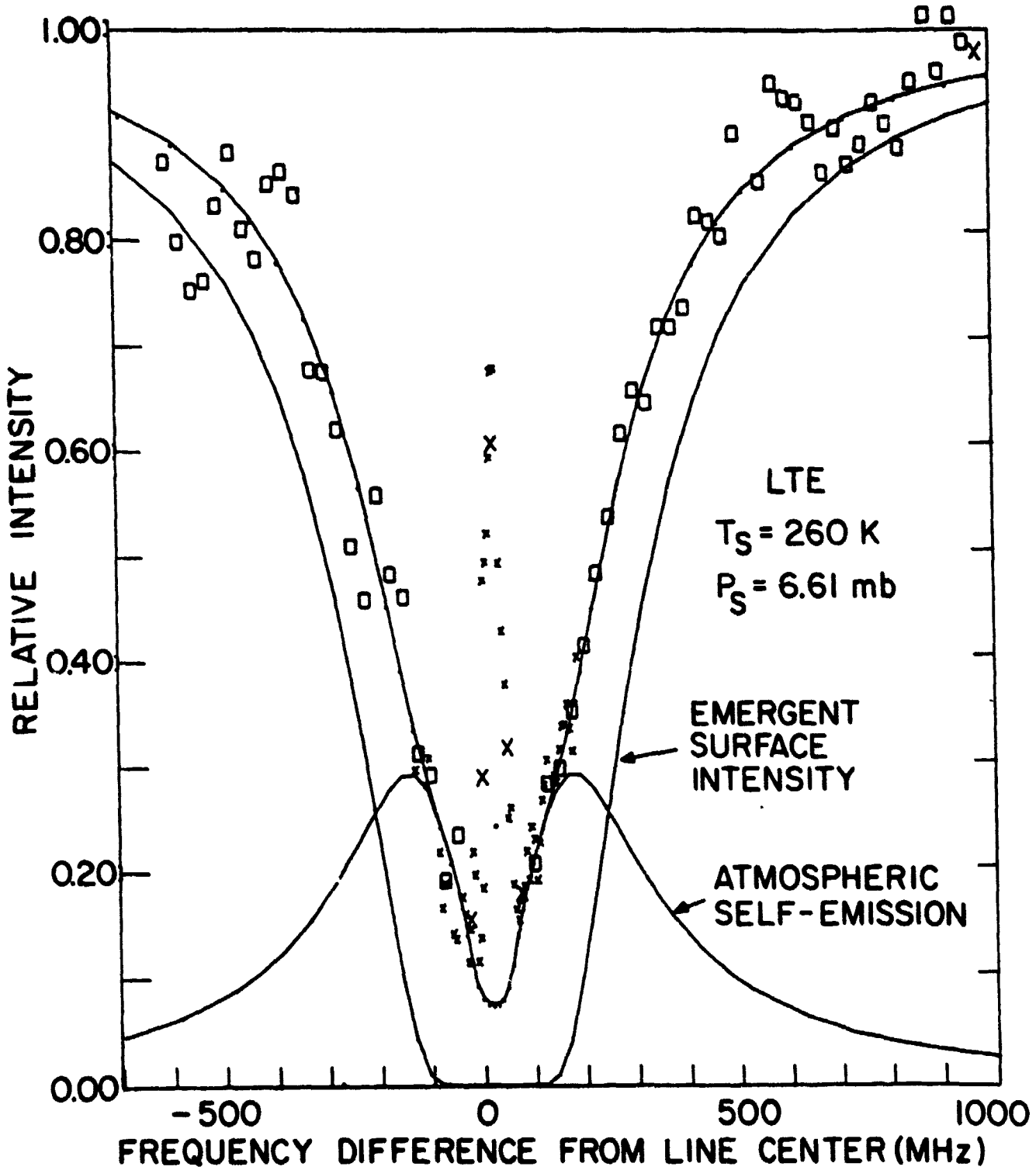
MARS - CO_2 R8
CML 41°
1.00
0.80
0.60
0.40
0.20
0.00
RELATIVE INTENSITY
LTE
T_S = 260 K
P_S = 6.61 mb
EMERGENT SURFACE INTENSITY
ATMOSPHERIC SELF-EMISSION
-500
0
500
1000
FREQUENCY DIFFERENCE FROM LINE CENTER (MHz)

FIGURE 3a

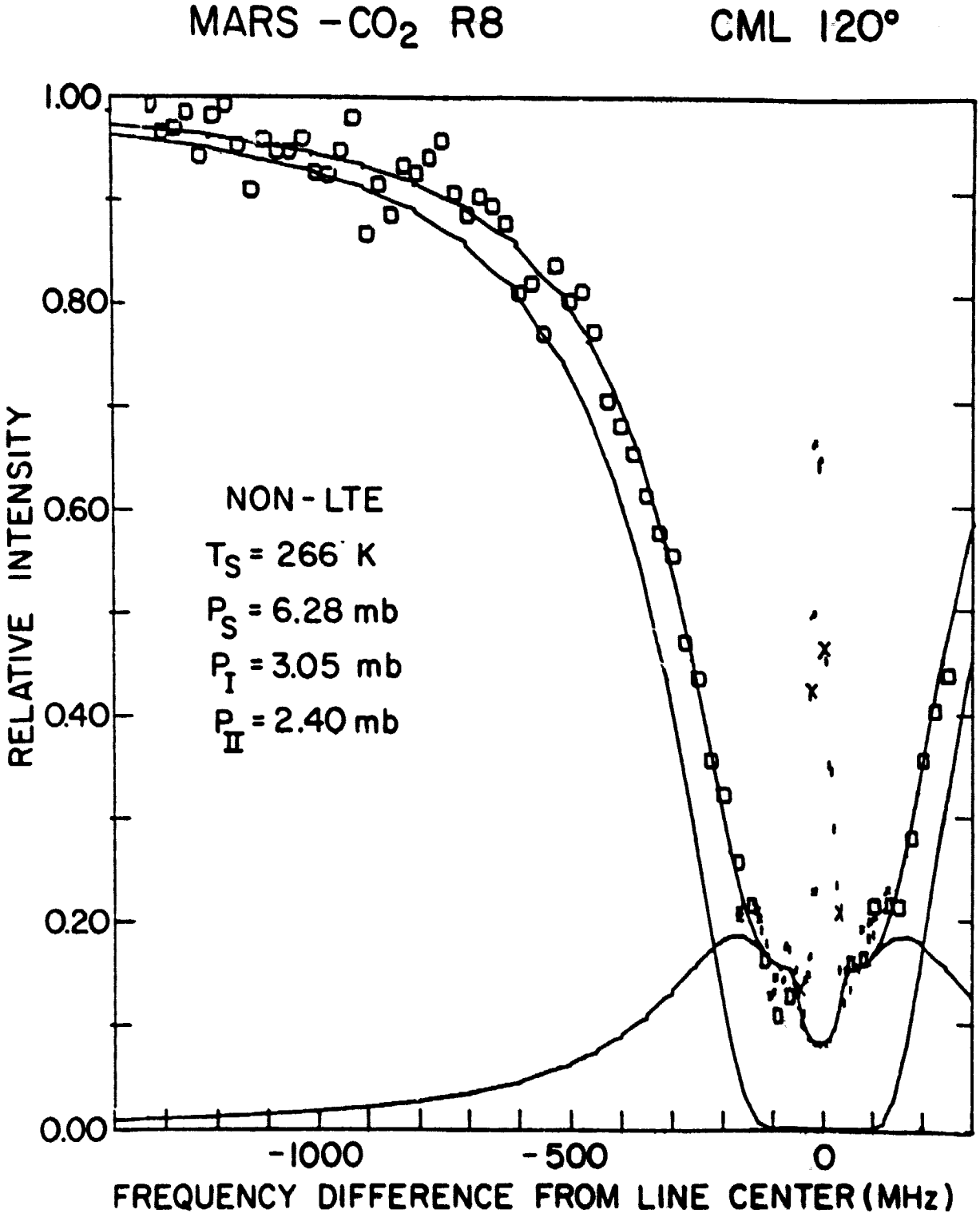
MARS - CO_2 R8
CML 120°
1.00
0.80
0.60
0.40
0.20
0.00
RELATIVE INTENSITY
NON - LTE
T_S = 266 K
P_S = 6.28 mb
P_I = 3.05 mb
P_{II} = 2.40 mb
-1000
-500
0
FREQUENCY DIFFERENCE FROM LINE CENTER (MHz)

FIGURE 3b

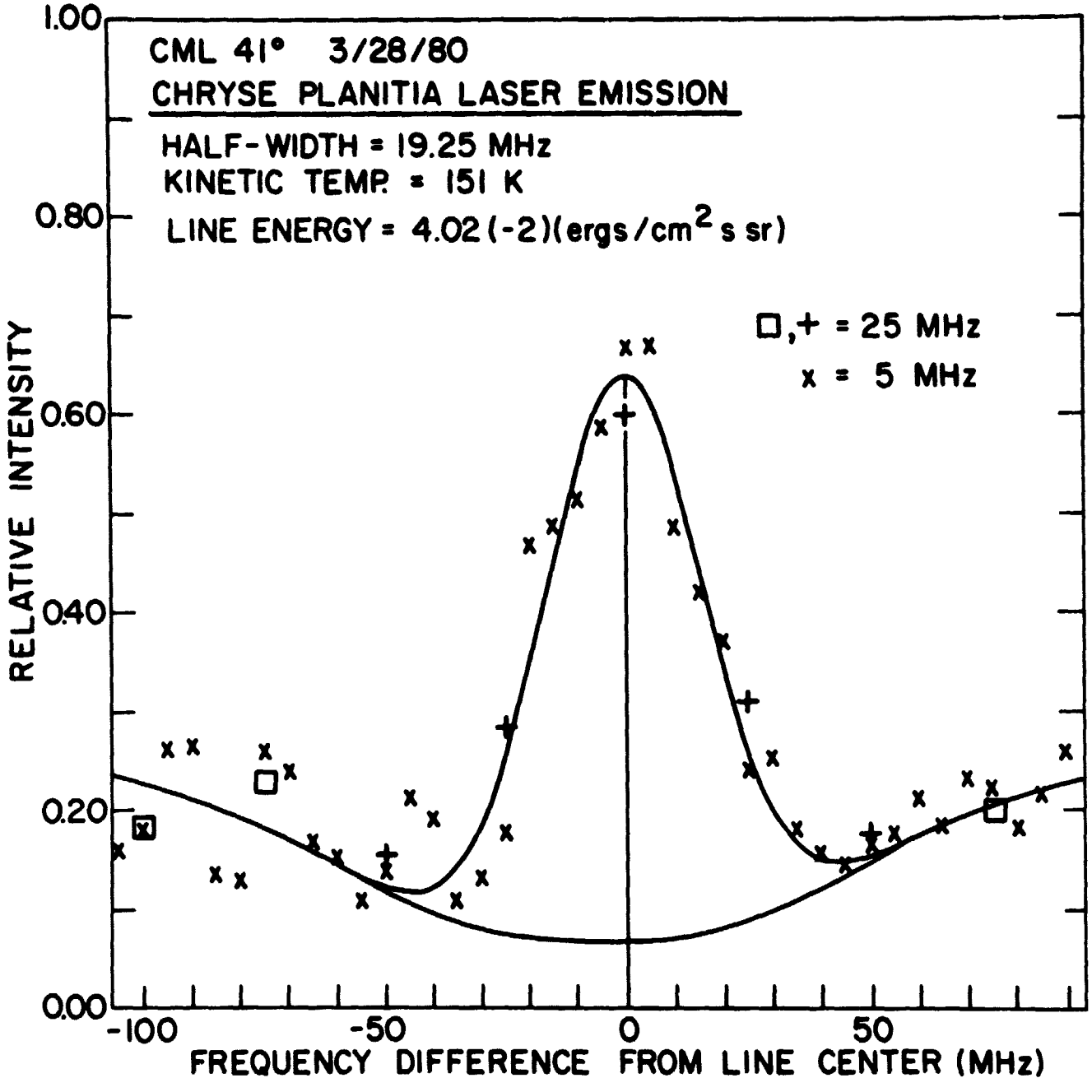
CML 41° 3/28/80
CHRYSE PLANITIA LASER EMISSION
HALF-WIDTH = 19.25 MHz
KINETIC TEMP. = 151 K
LINE ENERGY = 4.02(-2)(ergs/cm^2 s sr)
□,+ = 25 MHz
x = 5 MHz
RELATIVE INTENSITY
1.00
0.80
0.60
0.40
0.20
0.00
-100
-50
0
50
FREQUENCY DIFFERENCE FROM LINE CENTER (MHz)

FIGURE 4a

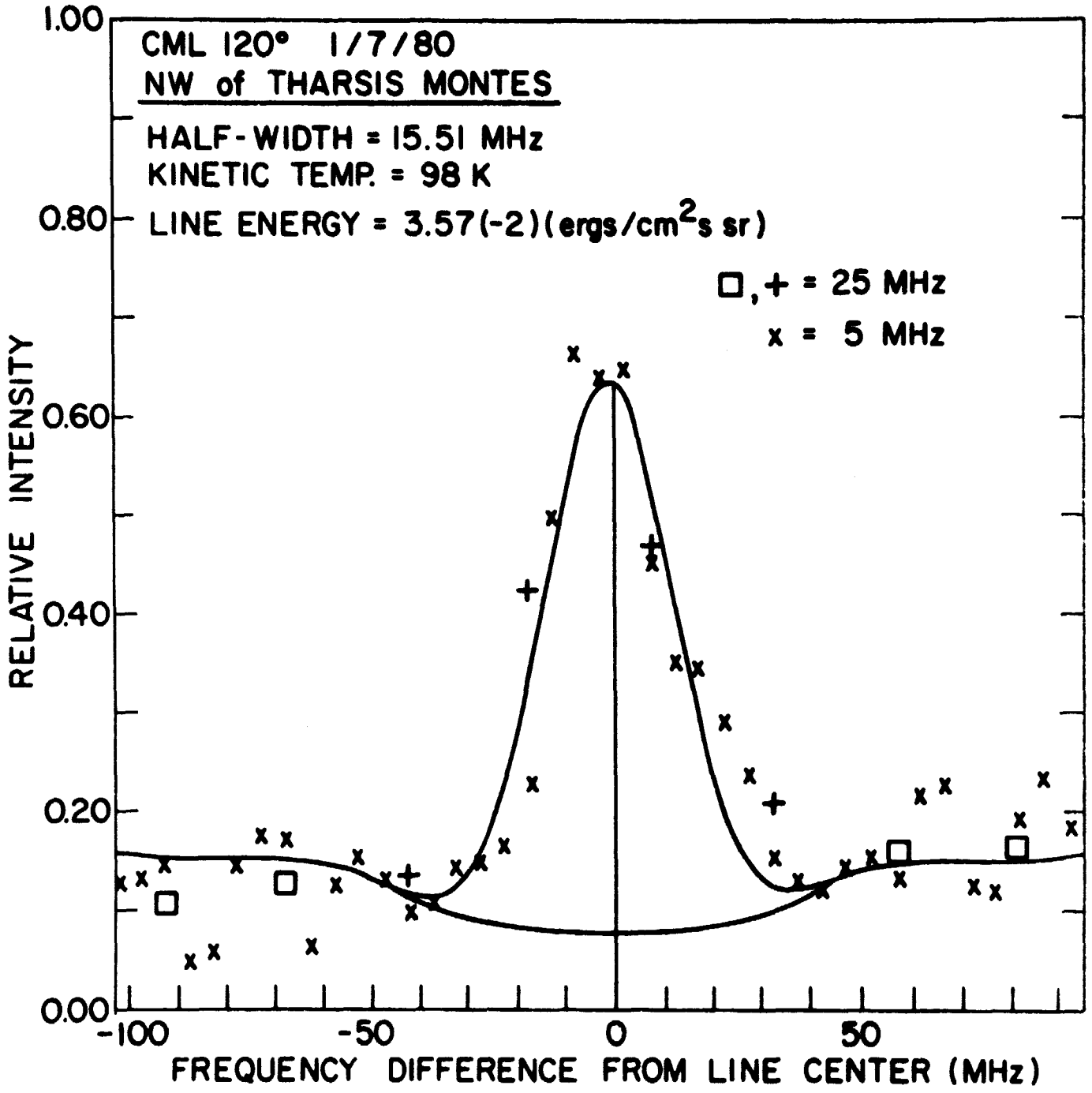
CML 120° 1/7/80
NW of THARSIS MONTES
HALF-WIDTH = 15.51 MHz
KINETIC TEMP. = 98 K
LINE ENERGY = 3.57(-2)(ergs/cm²s sr)
□,+ = 25 MHz
x = 5 MHz
RELATIVE INTENSITY
1.00
0.80
0.60
0.40
0.20
0.00
-100
-50
0
50
FREQUENCY DIFFERENCE FROM LINE CENTER (MHz)

FIGURE 4b